Hepatic Medicine: Evidence and Research

Dovepress
Taylor & Francis Group

Open Access Full Text Article

ORIGINAL RESEARCH

Identification of Ferroptosis -Related Genes in MAFLD/MASH and HQHF Validation

Sutong Liu[1–3,*], Lihui Zhang[1–3,*], Junjiao Xu[1], Qing Zhao[1], Dongfang Shang[1], Xiaoyan Liu[1], Qiang Zhang[1], Minghao Liu[1–3], Wenxia Zhao[1–3]

[1]The First Affiliated Hospital of Henan University of Chinese Medicine, Zhengzhou, 450000, People's Republic of China; [2]Collaborative Innovation Center of Prevention and Treatment of Major Diseases by Chinese and Western Medicine, Henan Province, Zhengzhou, 450000, People's Republic of China; [3]Collaborative Innovation Center of Research and Development on the Whole Industry Chain of Yu-Yao, Henan Province, Zhengzhou, 450000, People's Republic of China

*These authors contributed equally to this work

Correspondence: Minghao Liu; Wenxia Zhao, Email liumh015@163.com; qingteng1026@126.com

Video abstract

Point your SmartPhone at the code above. If you have a QR code reader the video abstract will appear. Or use: https://youtu.be/himtTuDV1UI.

Purpose: Metabolic associated fatty liver disease (MAFLD) and its progressive form, Metabolic Dysfunction-Associated Steatohepatitis(MASH), are prevalent liver disorders with significant health implications. This study aims to identify differentially expressed genes (DEGs) associated with MAFLD/MASH and explore their potential link to ferroptosis, a form of regulated cell death.

Methods: We conducted differential expression analysis using two datasets from the GEO database. Genes related to ferroptosis were identified from the Genecards and FerrDb databases, and the intersection genes were obtained by intersecting the DEGs with ferroptosis-related genes. Functional enrichment was performed using GO and KEGG pathways. The clinical diagnostic value of the intersection genes was evaluated through ROC analysis. Finally, the research findings were validated using a high-fat diet (HFD) mouse model, observing the improvement in gene expression with HQHF treatment.

Results: We utilized two datasets, GSE89632 and GSE63067, from the GEO database, comprising 39 samples, including 24 healthy controls. Differential expression analysis revealed significant gene expression changes in NAFLD and NASH compared to healthy controls. These DEGs were visualized using volcano plots. Ferroptosis-related genes were identified from Genecards and FerrDb databases, resulting in 1937 unique genes. Venn analysis revealed intersections between DEGs and ferroptosis genes, highlighting potential regulatory roles. Functional enrichment analysis using GO and KEGG pathways indicated significant involvement in cellular components and signaling pathways, such as PPAR and HIF-1. The clinical diagnostic value of intersecting genes was assessed using ROC analysis, demonstrating promising diagnostic potential. In addition, a high-fat diet (HFD) mouse model was used to validate the research findings, showing that HQHF treatment can alleviate lipid deposition and inflammation in the liver. Transmission electron microscopy results indicated that HQHF prevented mitochondrial damage and significantly reduced the content of Fe2+ in the liver, alleviating iron deposition. We verified the reliable genes with diagnostic value through qPCR, and the results suggested that HQHF can lower the transcription levels of P4HA1, NR4A1, and EFEMP1, while increasing the transcription levels of ENo3, GRIA3, ME1, and FADS2, confirming our ROC results.

Conclusion: This study provides insights into the molecular mechanisms underlying MAFLD/MASH and suggests ferroptosis-related genes as potential diagnostic biomarkers and therapeutic targets. Further research is warranted to explore these findings in clinical settings.

Keywords: metabolic associated fatty liver disease, ferroptosis, HQHF

Introduction

Metabolic associated fatty liver disease (MAFLD) is the most common chronic liver disease globally, affecting approximately 25% of adults, with an increasing incidence each year.[1] Metabolic Dysfunction-Associated Steatohepatitis(MASH) is a progressive form of MAFLD, affecting 20–30% of MAFLD patients.[2] The molecular mechanisms of MASH are closely related to hepatocyte injury, fibrosis, and inflammation, indicating that its pathological state is more severe than that of

Received: 13 December 2024
Accepted: 29 April 2025
Published: 2 May 2025

MAFLD.[1] Current treatment strategies for MAFLD mainly focus on lifestyle changes, such as weight loss and dietary adjustments, which have shown histological improvements in some cases.[3] However, options for pharmacological treatment remain limited, with only a few drugs like pioglitazone and vitamin E showing efficacy in specific patient populations.[4] In the treatment of MASH, the Resmenntiron approved by the US Food and Drug Administration has shown certain efficacy in treating MASH and liver fibrosis.[5] Despite these efforts, there is an urgent need for new therapeutic approaches and biomarkers to aid in the early diagnosis and management of these diseases.

Ferroptosis is a novel form of non-apoptotic cell death.[6] Iron deposition, damage to the antioxidant system, lipid oxidative stress response, and mitochondrial metabolic disorders are key biochemical processes that induce iron death, playing an important role in liver system diseases. The mechanism of Ferroptosis has been partially elucidated: first, iron overload can generate a large number of free radicals through the Fenton reaction, leading to oxidative stress, which is the main reason for the progression from simple fatty liver to MASH.[7] Second, a large amount of the antioxidant glutathione (GSH) is consumed by lipid peroxides and hydrogen peroxides, resulting in the inactivation of glutathione peroxidase 4 (GPx4). The depletion of GSH and the inactivation of GPx4 are considered necessary factors that promote lipid peroxidation in the process of Ferroptosis.[8] Additionally, oxidative stress can produce a large number of lipid peroxidation products such as 4-hydroxynonenal (4-HNE) and malondialdehyde (MDA), as well as various oxidized and modified proteins.[9] These products can lead to the destruction of the structural integrity of hepatocyte membranes, resulting in hepatocyte death.[10]

Ferroptosis is associated with various cellular processes, including oxidative stress and inflammation, both of which are critical in the progression of liver diseases.[11] However, the specific involvement of ferroptosis-related genes and their contributions to MAFLD and MASH remain insufficiently understood and warrant further exploration.

The Huatan Qushi Huoxue prescription (HQHF)is a traditional Chinese medicine compound that has been confirmed through extensive clinical and basic research to have significant efficacy in treating MAFLD/MASH.[12–15] In a high-fat diet mouse model, we also found that it inhibits the occurrence of the ferroptosis phenotype, but the specific connections with ferroptosis-related genes have not been thoroughly investigated, which merits further research.

This study employs a multidisciplinary approach, combining bioinformatics analysis, animal models, and molecular biology techniques to investigate the involvement of ferroptosis in MAFLD and MASH. By analyzing gene expression profiles and identifying differentially expressed genes associated with ferroptosis, we explore potential therapeutic targets through the intervention effects of the Phlegm-resolving, Dampness-dispelling, and Blood-activating formula. Additionally, this study aims to identify potential biomarkers for MAFLD and MASH to facilitate early diagnosis and therapeutic intervention.

Materials and Methods

Data Set Acquisition

Download the expression matrices, gene lists, and sample information for datasets GSE89632 and GSE63067 from the GEO (https://www.ncbi.nlm.nih.gov/geo/) database. These two datasets include 39 samples, 24 healthy controls, 11 samples, and 7 healthy controls.

Acquisition of Ferroptosis-Related Genes

Retrieve ferroptosis genes from the Genecards (https://www.genecards.org/) database, adjusting the threshold to score ≥ 2 for screening. Download ferroptosis genes from http://www.zhounan.org/ferrdb/current/. After merging the two datasets and removing duplicates, a total of 1937 ferroptosis genes are obtained.

Differential Expression Analysis

We used R (4.2.1) software for subsequent analysis. The normalizeBetweenArrays function from the limma package was used to normalize the data and perform differential analysis, with the results visualized using the ggplot2 package. The threshold screening criteria were $|\text{Log2(fold change)}| \geq 0.5$ and p-value < 0.05. Upregulated and downregulated genes

were intersected with ferroptosis genes, and the results were visualized using the ggplot2 and VennDiagram packages. We also used the ComplexHeatmap package to visualize significantly expressed molecules with heatmaps.

Functional Enrichment Analysis

We first used the org.Hs.eg.db package for ID conversion of the molecular list, and then performed enrichment analysis using the clusterProfiler package, selecting Homo sapiens as the species.

Clinical Diagnostic Value Analysis

ROC analysis was conducted on the intersected genes using the pROC package, and the results were visualized with the ggplot2 package.

Animal Rearing and MAFLD Model Construction

The animals used in this study were ordered from Zhejiang Weitong Lihua Experimental Animal Technology Co., Ltd., and the quality of the animals was qualified. The animal research protocol for this study has been approved by the Ethics Committee of Henan University of Traditional Chinese Medicine, and all experimental procedures were conducted according to ethical standards. Male C57BL/6 mice, 6 weeks old, weighing 20–25 g, were selected. All mice were housed under a 12-hour light/dark cycle in a pathogen-free environment, with a controlled temperature of 23 ± 2 °C and humidity of 60 ± 5%, with free access to food and water.

The mice were randomly divided into three groups: control, high-fat group, and drug intervention group, with 10 mice in each group. The high-fat and drug intervention groups were fed a high-fat diet (84% basic feed + 1% cholesterol + 10% lard + 5% egg yolk powder), while the control group was given regular feed. The drug intervention group received drug gavage for 4 weeks after 8 weeks of high-fat feeding.

Drug Preparation and Gavage

HQHF is procured from the First Affiliated Hospital of Henan University of Traditional Chinese Medicine. Each prescription contains Alisma 30g, Seaweed 15g, Cassia Seed 10g, Aromatic Turmeric 15g, Danshen 15g, Hawthorn 15g, Bupleurum 6g, Silybum marianum 15g. The total daily dosage for adults is 121g. Based on the conversion factor of 9.01 for a 60kg adult to mouse dosage, the herbs are soaked in advance for 30 minutes, using a 1:10 ratio in a multifunctional barrel for 30 minutes. After heating and filtering, a decoction is obtained, which is then concentrated to 360 mL using a rotary evaporator, shaken well, and prepared as HQHF.

Orbitrap High-Resolution Liquid Chromatography-Mass Spectrometry Analysis

100 μL of the Chinese medicine decoction was mixed with 300 μL of methanol, vortexed, centrifuged, and the supernatant was evaporated before analysis. Data was initially organized using CD 3.3 (Compound Discoverer 3.3) (Thermo Fisher) and then searched against the mzCloud database for comparison.

Total RNA Extraction and Real-Time Quantitative PCR

20 mg of liver tissue was added to 1 mL of RNA extraction solution for RNA extraction. Reverse transcription was completed using a reverse transcription kit (Catalog No.: G3337) on a standard PCR machine. Amplification was performed on a fluorescent quantitative PCR machine. GAPDH was used as the internal reference gene, and the relative expression level of genes was quantified using the 2[–ΔΔCt] method. Primer sequences are provided in Table 1

Determination of Ferrous Ion by Colorimetric Method

The kit was obtained from Elabscience, product number: E-BC-K773-M. Prepare standard and measurement tubes, dilute the sample 2-fold with 300 μL, and add the color development solution, centrifuging for 10 minutes. The supernatant was added to a microplate, and the OD value of each well was measured at 593 nm using a microplate reader.

Table 1 The Sequence of the Primer

PPrimer Information	Primer Name	Primer Sequence (5′-3′)R-Efemp1-S R-Efemp1-A	Segment Length (bp)	Annealing Temperature (°C)
NM_017008.4	R-GAPDH-S	CTGGAGAAACCTGCCAAGTATG	138	60
	R-GAPDH-A	GGTGGAAGAATGGGAGTTGCT		60
NM_172062.2	R-P4ha1(2)-S	CTTCTTGAACTAGATCCTGAACACC	162	60
	R-P4ha1(2)-A	TGGCAGGTAGTCCACAGCAAT		60
NM_024388.2	R-NR4A1-S	TTGGAAAGGAAGATGCCGG	270	60
	R-NR4A1-A	TGTCTATCCAGTCACCAAAGCC		60
NM_012949.2	R-Eno3-S	CCACGGGTATCTATGAAGCACTG	192	60
	R-Eno3-A	ACTTATTCTCGGTTCCGTCCAG		60
NM_001112742.1	R-Gria3-S	ACCATCAGCATAGGTGGACTTT	106	60
	R-Gria3-A	GCTTCTCAGTGGTGTTCTGGTTG		60
NM_012600.3	R-Me1-S	CAAAGGGCATATTGCTTCAGTTCT	178	60
	R-Me1-A	ACACTGTTGTGGATTCACCCCTC		60
NM_001012039.1	R-Efemp1-S	AAATAACTTCGTCATTCGGAGGAA	231	60
	R-Efemp1-A	TGTTCGCCTCGCTTCTGATA		60
NM_031344.2	R-Fads2-S	AGATTGAGCACCACCTCTTCCC	102	60
	R-Fads2-A	CTTGGTATTCAATGCCATGCTT		60

HE Staining

Frozen sections were thawed, fixed, and pretreated. Staining was performed using hematoxylin and eosin. Finally, dehydration and mounting were done.

Oil Red O Staining

Frozen sections were removed, thawed, fixed, washed with water, and dried. The prepared Oil Red O staining solution was left to stand overnight, filtered three times, and the sections were stained. Isopropanol differentiation and washing were performed. Hematoxylin dye was used for staining, followed by mounting.

Transmission Electron Microscopy

Fresh tissue was cut into approximately 1 mm pieces, sampled within 1–3 minutes, quickly placed in electron microscopy fixative, embedded, ultrathin sections were prepared, and stained with lead and uranium, followed by negative staining.

Statistical Analysis

All results are expressed as mean ± standard deviation (M ± SEM). Statistical analysis was performed using GraphPad Prism 9.5. Charts were created using R (4.2.1) version.

Ethics Approval

The research protocol was approved by the Ethics Committee of Henan University of Traditional Chinese Medicine. Specifically, we follow the "Guidelines for the Ethical Review of Animal Welfare in Experiments in China (2018 Edition)" which was issued by the General Administration of Quality Supervision, Inspection and Quarantine of the People's Republic of China and the National Standardization Administration of China.

Results

Identification of Differential Genes in NAFLD/NASH

This study selected two datasets, GSE89632 and GSE63067. GSE89632 includes 20 cases of NAFLD, 19 cases of NASH, and 24 healthy liver samples. GSE63067 includes 2 cases of NAFLD, 9 cases of NASH, and 7 healthy liver

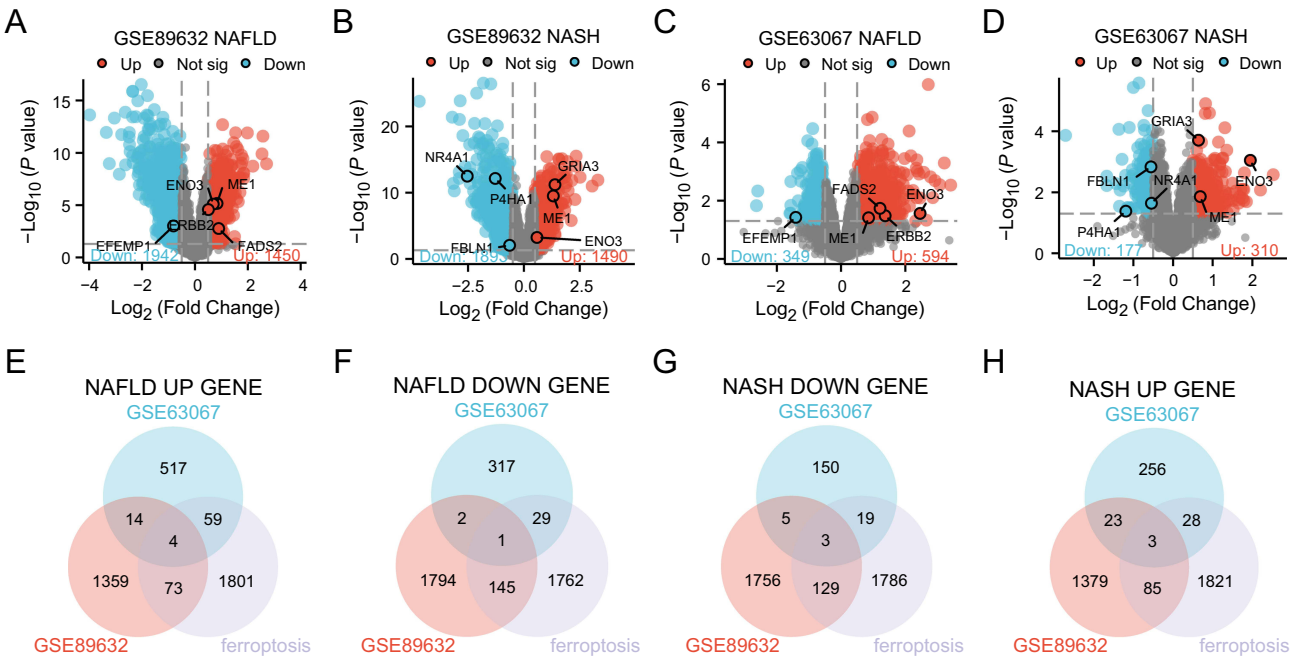

Figure 1 Identification of Differential Genes in NAFLD/NASH. Differential genes of NAFLD shown in (**A**) for GSE89632, differential genes of NASH shown in (**B**) for GSE89632, differential genes of NAFLD shown in (**C**) for GSE63067, differential genes of NASH shown in (**D**) for GSE63067, the intersection of upregulated genes in NAFLD and ferroptosis genes shown in (**E**), the intersection of downregulated genes in NAFLD and ferroptosis genes shown in (**F**), the intersection of downregulated genes in NASH and ferroptosis genes shown in (**G**), the intersection of upregulated genes in NASH and ferroptosis genes shown in (**H**).

samples. After conducting a differential analysis on the GSE89632 dataset, we found that 1450 genes were upregulated and 1942 genes were downregulated in NAFLD compared to healthy controls; in NASH compared to healthy controls, 1490 genes were upregulated and 1893 genes were downregulated. In the GSE63067 dataset, 594 genes were upregulated and 349 genes were downregulated in NAFLD compared to healthy controls; in NASH compared to healthy controls, 310 genes were upregulated and 177 genes were downregulated. These results were visualized using volcano plots, which show each plot representing a gene, with blue indicating downregulation and red indicating upregulation (Figure 1A–D). We identified 1546 ferroptosis genes from the Genecards database, and 834 ferroptosis genes were downloaded from the http://www.zhounan.org/ferrdb/current/database. After merging and removing duplicates, we obtained a total of 1937 ferroptosis genes. We conducted a Venn analysis comparing the upregulated and downregulated genes with the ferroptosis genes. The results showed that there were 3 overlapping genes between NASH's upregulated genes and ferroptosis genes, and 3 overlapping genes among the downregulated genes; for NAFLD, there were 4 overlapping genes in the upregulated genes and 1 overlapping gene among the downregulated genes (Figure 1E–H).

Expression of Differential Genes

The expression matrix of differential genes was visualized, and the results indicated that the expression differences of these genes between the disease group and the healthy group were very significant (Figure 2A–D).

GO and KEGG Enrichment Analysis of Differentially Expressed Genes Related to Ferroptosis

Differentially expressed genes were subjected to KEGG and GO enrichment analysis. The results showed (Figure 3A and B) that the cellular components of ferroptosis-related DEGs included parallel fiber to Purkinje cell synapse, plasma membrane signaling receptor complex, AMPA glutamate receptor complex, collagen-containing extracellular matrix, and ionotropic glutamate receptor complex. The molecular functions mainly included: transmembrane receptor protein tyrosine kinase activity, transmembrane receptor protein kinase activity, protein tyrosine kinase activity, extracellular matrix structural constituent, and oxidoreductase activity acting on paired donors, with incorporation or reduction of

https://doi.org/10.2147/HMER.S509778

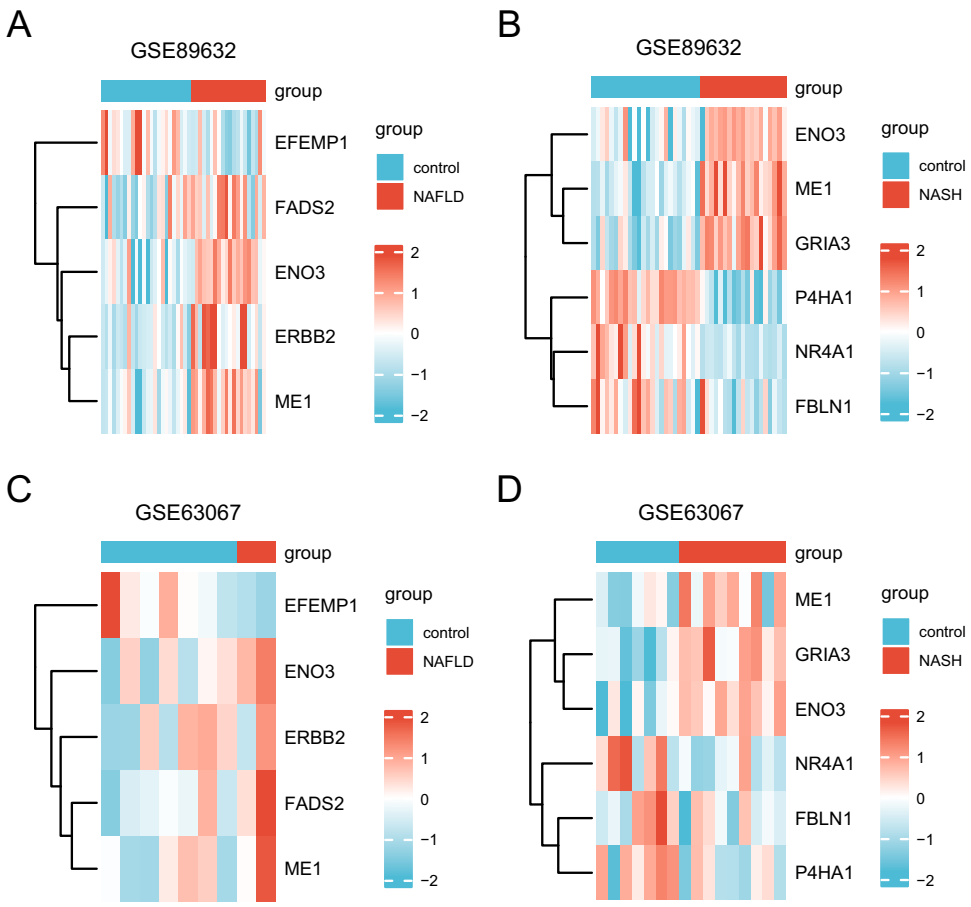

Figure 2 Expression of differential genes. The expression matrix of differential genes in different groups for GSE89632 NASH shown in (**A**), the expression matrix of differential genes in different groups for GSE89632 NAFLD shown in (**B**), the expression matrix of differential genes in different groups for GSE63067 NAFLD shown in (**C**), and the expression matrix of differential genes in different groups for GSE63067 NASH shown in (**D**).

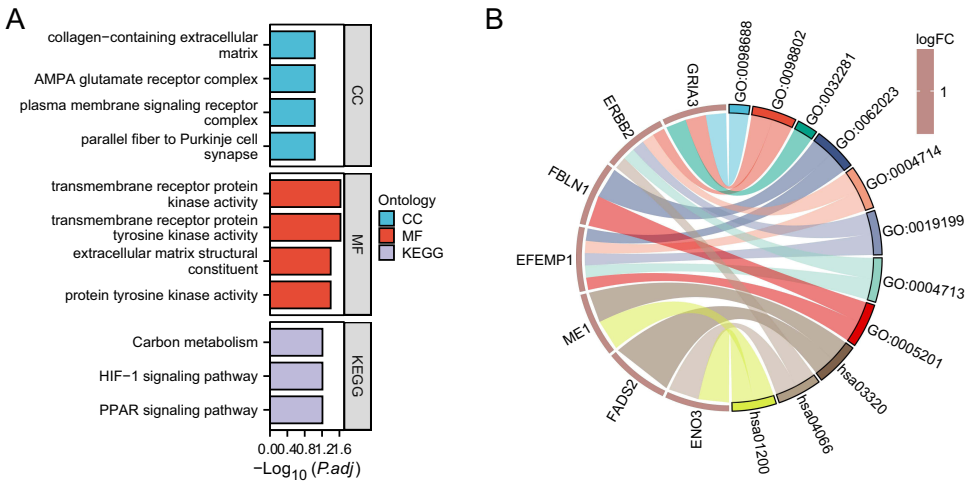

Figure 3 GO and KEGG enrichment analysis of differentially expressed genes related to ferroptosis. The bar chart of GOKEGG analysis results of differentially expressed genes shown in (**A**), and the chord diagram of GOKEGG combined with logFC analysis shown in (**B**).

molecular oxygen. In the KEGG enrichment analysis, the main enriched pathways included the PPAR signaling pathway, HIF-1 signaling pathway, and carbon metabolism.

Prognostic Value of Differential Genes

We plotted the ROC curves of 11 differential genes based on the expression levels from the GSE89632 and GSE63067 datasets to validate their distinguishing role between NAFLD/NASH patients and healthy controls. The results showed (Figure 4A–D) that in the GSE89632 dataset, the area under the ROC curve for the 5 hUP genes related to NAFLD demonstrated good diagnostic performance. In the GSE63067 dataset, the area under the ROC curve for the 5 hUP genes related to NAFLD showed that only the result for ERBB2 was less than 0.75, while the other 4 genes exhibited good diagnostic value. In the GSE89632 dataset, the area under the ROC curve for the 6 hUP genes related to NASH also showed good diagnostic performance. In the GSE63067 dataset, the area under the ROC curve for the 6 hUP genes related to NAFLD showed that only the result for FBLN1 was less than 0.75, while the other 5 genes exhibited good diagnostic value.

Analysis of the Main Components of HQHF

Qualitative identification of the main chemical components of the HQHF was conducted through Q-Orbitrap analysis. Figure 5 shows the total ion flow diagram for the identification of chemical components.

Drug Intervention in HFD Mouse Model

To establish the NAFLD model, we used C57BL/6 mice and fed them a high-fat diet (84% basic feed + 1% cholesterol + 10% lard + 5% egg yolk powder) for 12 weeks. We observed a significant increase in body size and weight in HFD-fed mice compared to the control group. Mice undergoing drug intervention were smaller in size compared to HFD mice. The weight gain in HFD mice was more pronounced, while the weight of drug intervention mice showed a gradual decline. Additionally, images of the livers from HFD mice displayed hepatomegaly, a pale appearance, and significant lipid accumulation. In contrast, the livers of control group mice were smaller, with a dark red color and no signs of lipid accumulation observed. (Figure 6A–F).

Expression and Drug Validation of Ferroptosis-Related Genes in HFD Mouse Model

HE results of the liver showed significant hepatic steatosis and hepatocyte swelling in HFD mice, with destruction of liver tissue structure and visible inflammatory cells. HQHF could partially reverse the hepatic steatosis and inflammatory response in HFD-fed mice. Oil Red O staining revealed significant lipid degeneration in hepatocytes of HFD mice, with many spherical lipid droplets stained red, indicating obvious lipid accumulation in the liver. In the HQHF group, the number of lipid droplets in hepatocytes was significantly lower than that in the HFD group, showing changes similar to those in the blank group animals (Figure 7A and B).

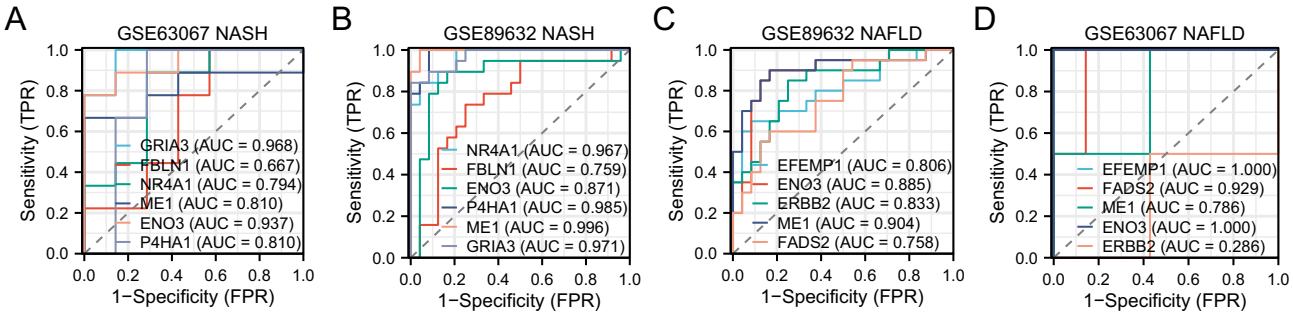

Figure 4 Prognostic Value of Differential Genes. The area under the ROC curve of differential genes in GSE63067 NASH shown in (**A**), the area under the ROC curve of differential genes in GSE89632 shown in (**B**), the area under the ROC curve of differential genes in GSE89632 NAFLD shown in (**C**), and the area under the ROC curve of differential genes in GSE63067 NAFLD shown in (**D**).

https://doi.org/10.2147/HMER.S509778

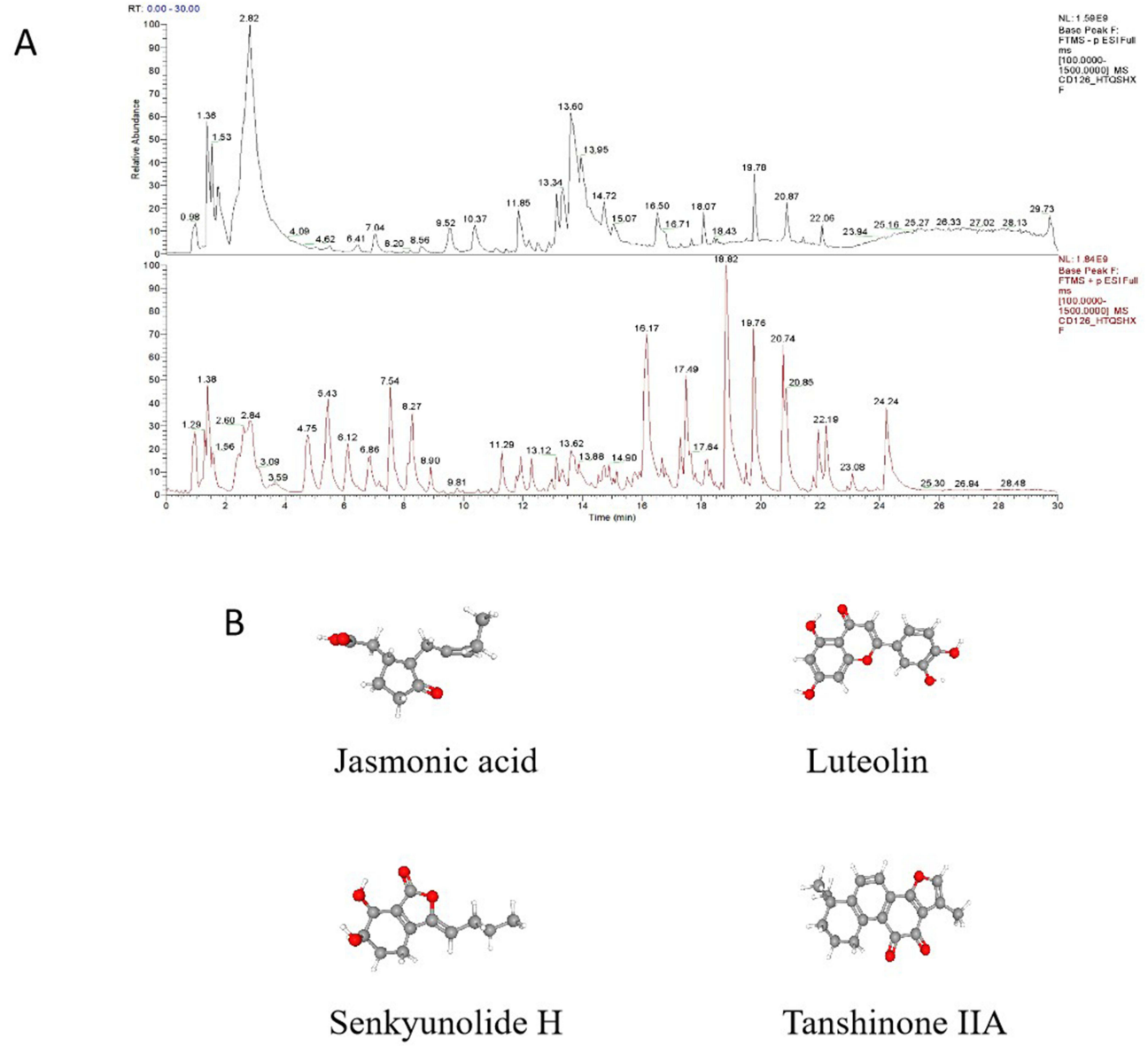

Figure 5 Analysis of the main components of HQHF. (**A**) Total ion flow diagram of the chemical composition identification of HQHF. (**B**) Structural formula of the main compound.

To verify the ferroptosis phenotype in HFD mice, we performed transmission electron microscopy on the liver, which showed that the nuclei of liver cells in HFD mice were round, with visible nucleoli, swollen mitochondria, blurred membrane structures, sparse matrix, and broken mitochondrial cristae, along with the presence of autophagy. In the HQHF group, the mitochondrial membrane structure was clear, and the morphology of mitochondria was similar to that of the blank group. Compared to the Fe2+ content in the livers of HFD group mice, HQHF can significantly reduce the Fe2+ content in the liver and alleviate iron deposition.(Figure 7D) To further validate the differential gene expression and drug verification in the HFD mouse model, we collected total RNA from three groups of liver tissues: blank group, HFD group, and HQHF group, with six mice in each group. Subsequent qRT-PCR analysis confirmed our ROC results (Figure 7E).

Discussion

MAFLD) and its more severe form—MASH)—represent an increasingly serious global health issue.[16] These diseases are associated with metabolic syndrome and may progress to liver fibrosis, cirrhosis, and hepatocellular carcinoma.[17] The

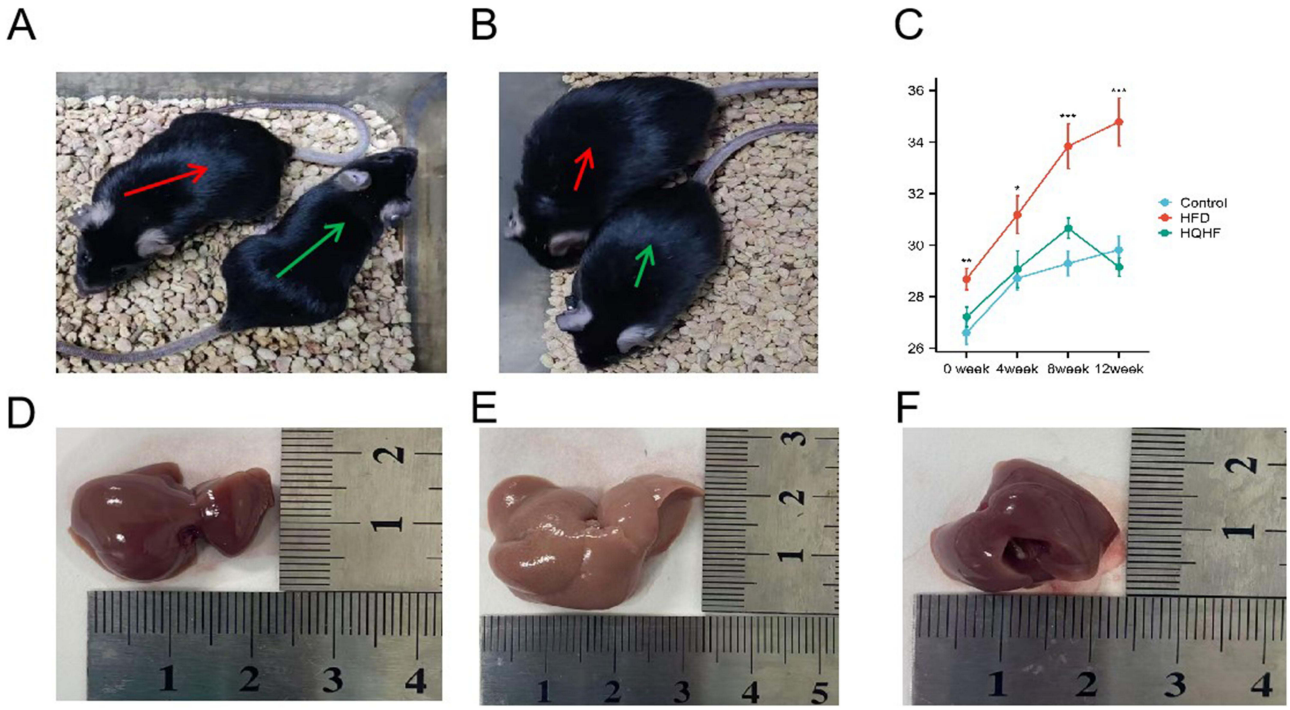

Figure 6 Drug Intervention in HFD Mouse Model. (**A**) Shows mice fed with regular feed, while the left side shows the HFD group. The left side of (**B**) is the HFD group, and the right side is the HQHF group. (**C**) Shows the weight changes of mice in each group. (**D**) Shows the liver of the control group mice, (**E**) Shows the liver of the HFD group mice, and (**F**) shows the liver of the HQHF mice.

rising incidence of MAFLD/MASH is a growing concern, particularly as it correlates with increasing obesity rates and sedentary lifestyles. Understanding the molecular mechanisms underlying these diseases is crucial for developing effective treatment strategies.[18] This study aims to identify differentially expressed genes associated with MAFLD and MASH, focusing on the role of ferroptosis-related genes.

In this study, we utilized two datasets, GSE89632 and GSE63067, for a comprehensive analysis of gene expression profiles. The results showed a significant number of upregulated and downregulated genes in both NAFLD and NASH compared to healthy controls. Specifically, GSE89632 revealed 1450 upregulated genes and 1942 downregulated genes in NAFLD, while NASH exhibited 1490 upregulated genes and 1893 downregulated genes. Similarly, GSE63067 identified 594 upregulated genes and 349 downregulated genes in NAFLD, and 310 upregulated genes and 177 downregulated genes in NASH. The use of volcano plots effectively visualized these results, highlighting the expression differences between the disease groups and the control group.

Ferroptosis is a specific mode of cell death characterized by the continuous accumulation of lipid peroxides within the cells. In recent years, research in the scientific community has gradually revealed that iron death may play a crucial role in the pathogenesis of MAFLD.[19] Studies have shown that iron death is closely related to oxidative stress responses and inflammatory responses in the liver, and it may also influence the pathological state of the liver by regulating the expression of related genes.[20] Therefore, a deeper exploration of the mechanisms of action of genes associated with iron death will greatly aid in providing new biomarkers and potential therapeutic targets for the early diagnosis and treatment of MAFLD.[21]

Furthermore, the intersection analysis of ferroptosis-related genes revealed interesting overlaps, with NASH showing three commonly upregulated and three downregulated genes, while NAFLD had four upregulated and one downregulated gene from the ferroptosis gene set. This suggests a potential link between ferroptosis and the pathogenesis of NAFLD/NASH, warranting further investigation into the roles of these genes in disease progression. Functional enrichment analysis of differentially expressed genes (DEGs) indicated significant involvement in various biological processes and

https://doi.org/10.2147/HMER.S509778

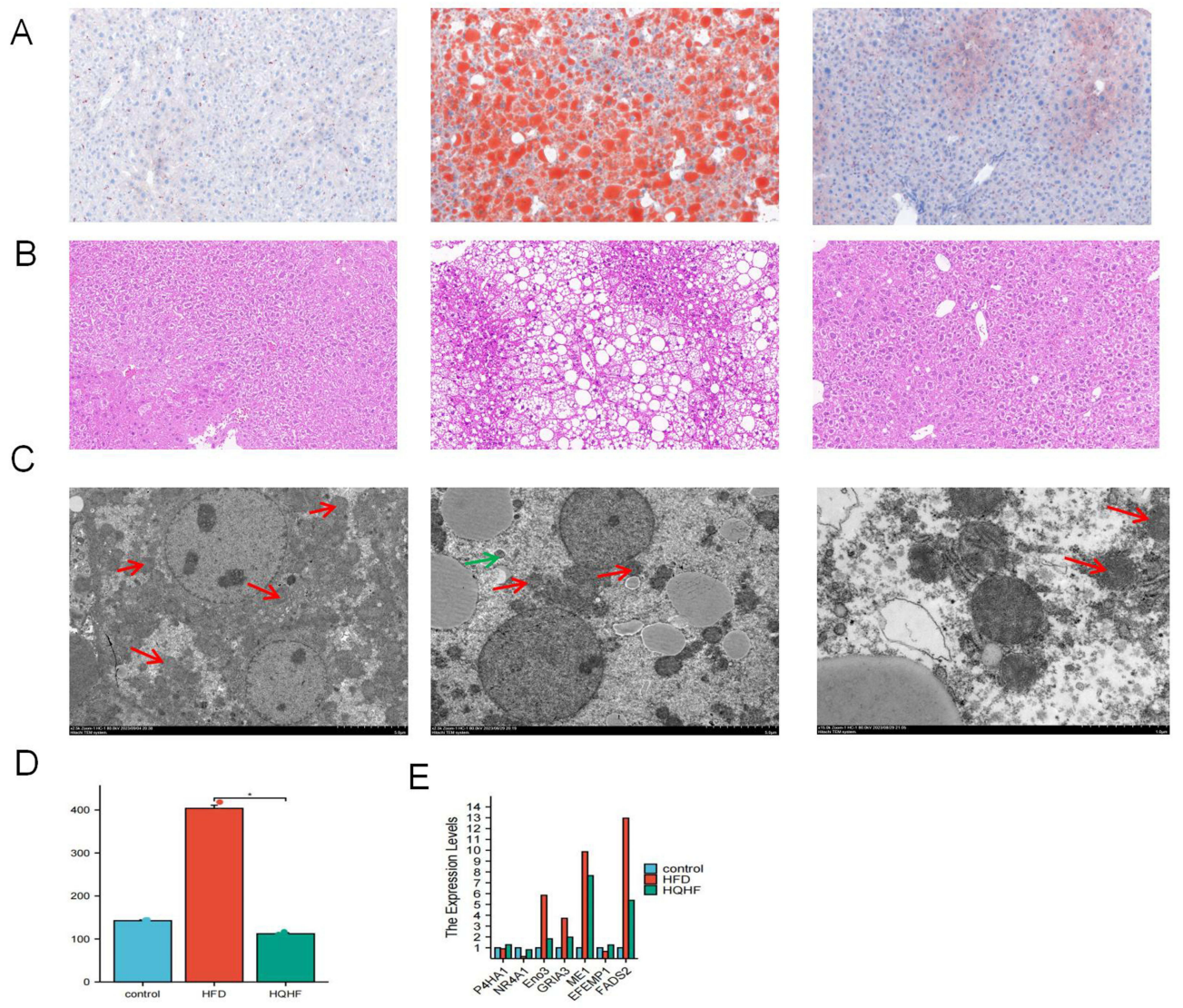

Figure 7 Expression and Drug Validation of Ferroptosis-Related Genes in HFD Mouse Model. (**A**) Oil red staining. (**B**) BHE staining. (**C**) Transmission electron microscopy. The red arrow refers to the structure of the mitochondria. (**D**) Fe2+ ion content. (**E**) qPCR results.

pathways, including the PPAR signaling pathway and HIF-1 signaling pathway, which are known to play key roles in lipid metabolism and cellular responses to hypoxia.

In addition, the ROC diagnostic results indicate that EFEMP1, ENo3, ME1, FADS2, GRIA3, NR4A1, and P4HA1 all demonstrate good diagnostic value. This further suggests that these ferroptosis-related genes may become biomarkers for MAFLD and MASH, thereby promoting the development of early diagnosis and treatment strategies.

Research shows that in the MASH mouse model induced by a high-fat diet, the protein level of EFEMP1 in liver tissue is elevated. After liver-specific AAV8-shEFEMP1 knockdown, the expression of the key factor for ferritin autophagy, NCOA4, is restored, promoting ferritin degradation and reducing free iron levels, which leads to a decrease in MDA levels in liver tissue and an increase in GPX4 activity.[22] In the db/db mouse model with a methionine-choline deficient (MCD) diet, the expression of ENO3 protein in liver tissue decreases. After tail vein injection of ENO3 overexpression adenovirus, mitochondrial lipid ROS levels are reduced, and ACSL4 protein levels decrease, improving the integrity of mitochondrial cristae.[23] In the SD rat model with a high fructose diet (HFrD, 30% fructose), a decrease in ME1 protein levels in liver tissue is observed. Specific knockout of liver ME1 using CRISPR/Cas9 technology can lead to NADPH depletion, GSH metabolic disorder, and induce ferroptosis.[24] In PA-induced

AML12 hepatocytes, FADS2 protein levels are elevated, and siRNA knockdown of FADS2 can reduce PUFA synthesis and alleviate lipid peroxidation. In the ApoE-/- mouse model induced by a high-fat high-cholesterol (HFHC) diet, GRIA3 protein in liver tissue is elevated.[25] Oral administration of the AMPA receptor antagonist Perampanel (3 mg/kg/d for 4 weeks) can maintain mitochondrial homeostasis: reducing ROS accumulation by decreasing mitochondrial membrane potential ($\Delta\Psi m$).[26] In the HFD+CCl4-induced mouse liver fibrosis model, the mRNA level of NR4A1 in liver tissue is elevated, and knockdown of NR4A1 can upregulate antioxidant genes: HO-1 levels, improving iron metabolism disorders and reducing non-transferrin bound iron (NTBI) in liver tissue.[27] The H2O2-induced hypoxia model in HepG2 cells simulates the NASH microenvironment, and after stable knockdown of P4HA1 with shRNA, HIF-1α is inhibited, reducing lipid droplet formation.[28]

Additionally, animal model experiments conducted under ethical approval further corroborated these findings, exploring the therapeutic potential of a phlegm-resolving, dampness-dispelling, and blood-activating formula, thereby bridging the gap between computational discoveries and in vivo applications. Overall, the application of these methodologies aids in a comprehensive understanding of the molecular mechanisms of MAFLD and MASH while highlighting potential therapeutic targets.

Conclusions

In summary, this result helps to provide references for the pathogenesis and treatment of MAFLD and MASH.

Data Sharing Statement

The disease dataset used in this article was downloaded from the GEO database, and the phenotypic genes were obtained from the Genecards (https://www.genecards.org/) database, http://www.zhounan.org/ferrdb/current/.

Acknowledgments

Thank all the authors of this article for their efforts, and thank the laboratory teacher Ma Qingliang for providing us with an experimental environment.

Author Contributions

All authors made a significant contribution to the work reported, whether that is in the conception, study design, execution, acquisition of data, analysis and interpretation, or in all these areas; took part in drafting, revising or critically reviewing the article; gave final approval of the version to be published; have agreed on the journal to which the article has been submitted; and agree to be accountable for all aspects of the work.

Funding

National Natural Science Foundation of China [No. 82205086], Science and Technology Key Project of Henan Province [No. 232102310438], and the 9th China Association for Science and Technology Young Talent Support Project [No. 2023QNRC001], Research project of Henan Province [2022JDZX114], Henan Province Traditional Chinese medicine "double first-class" to create a scientific research project [HSRP-DFCTCM-2023-5-13], Henan Province Postdoctoral Fund [HN2024080].

Disclosure

All authors declare no competing or conflicting interests in this work.

References

1. Targher G, Tilg H, Byrne CD. Non-alcoholic fatty liver disease: a multisystem disease requiring a multidisciplinary and holistic approach. *Lancet Gastroenterol Hepatol*. 2021;6(7):578–588. doi:10.1016/S2468-1253(21)00020-0
2. Papatheodoridi M, Cholongitas E. Diagnosis of Non-alcoholic Fatty Liver Disease (NAFLD): current concepts. *Curr Pharm Design*. 2018;24 (38):4574–4586. doi:10.2174/1381612825666190117102111
3. Roeb E. Excess body weight and metabolic (Dysfunction)-Associated Fatty Liver Disease (MAFLD). *Visc Med*. 2021;37(4):273–280. doi:10.1159/000515445

4. Diehl AM, Day C. Cause, pathogenesis, and treatment of nonalcoholic steatohepatitis. *New Engl J Med*. 2017;377(21):2063–2072. doi:10.1056/NEJMra1503519
5. Petta S, Targher G, Romeo S, et al. The first MASH drug therapy on the horizon: current perspectives of resmetirom. *Liver Int*. 2023;44(7):1526–1536. doi:10.1111/liv.15930
6. Stockwell BR. Ferroptosis turns 10: emerging mechanisms, physiological functions, and therapeutic applications. *Cell*. 2022;185(14):2401–2421. doi:10.1016/j.cell.2022.06.003
7. Czaja AJ. Review article: iron disturbances in chronic liver diseases other than haemochromatosis - pathogenic, prognostic, and therapeutic implications. *Aliment Pharmacol Ther*. 2019;49(6):681–701. doi:10.1111/apt.15173
8. Santana-Codina N, Gikandi A, Mancias JD. The role of NCOA4-mediated ferritinophagy in ferroptosis. *Adv Exp Med Biol*. 2021;1301:41–57. doi:10.1007/978-3-030-62026-4_4
9. Ajoolabady A, Aslkhodapasandhokmabad H, Libby P, et al. Ferritinophagy and ferroptosis in the management of metabolic diseases. *Trends Endocrinol Metab*. 2021;32(7):444–462. doi:10.1016/j.tem.2021.04.010
10. Wu CT, Deng JS, Huang WC, et al. Salvianolic Acid C against acetaminophen-induced acute liver injury by attenuating inflammation, oxidative stress, and apoptosis through inhibition of the Keap1/Nrf2/HO-1 signaling. *Oxid Med Cell Longev*. 2019;2019:9056845. doi:10.1155/2019/9056845
11. Tao L, Yang X, Ge C, et al. Integrative clinical and preclinical studies identify FerroTerminator1 as a potent therapeutic drug for MASH. *Cell Metab*. 2023;36(10):2190–2206.e5. doi:10.1016/j.cmet.2024.07.013
12. Liu S, Zhang L, Gu Y, et al. Effect of Huatan Qushi Huoxue prescription on the ultrastructure of hepatocyte mitochondria in rats with nonalcohol-ic steatohepatitis. *J Clin Hepatobiliary Dis*. 2022;38(08):1780–1783. doi:10.3969/j.issn.1001-5256.2022.08.012
13. Liu M, Liu S, Shang D, Zhang L, Gu Y, Zhao W. Effect of Huatan Qushi Huoxue prescription on lipopolysaccharide-induced pyroptosis of macrophages. *J Clin Hepatol*. 2022;38(09):2016–2019. doi:10.3969/j.issn.1001-5256.2022.09.014
14. Zhang L, Liu S, Zhang W, Zhang J, Zhao W. Mechanism of Huatan Qushi Huoxue Formula in improving the inflammatory injury of rats with nonalcoholic steatohepatitis based on ADPN/PI3K/AKT signal pathway. *Chin J Tradit Chin Med Pharm*. 2021;36(10):5832–5837.
15. Zhang L, Zhang J, Zhao W. Effect of Huatan Qushi Huoxue prescription on the key proteins of the ADPN/PI3 K/Akt signaling pathway in rats with nonalcoholic steatohepatitis. *J Clin Hepatol*. 2020;36(04):835–839. doi:10.3969/j.issn.1001-5256.2020.04.025
16. Kanda T, Matsuoka S, Yamazaki M, et al. Apoptosis and non-alcoholic fatty liver diseases. *World J Gastroenterol*. 2018;24(25):2661–2672. doi:10.3748/wjg.v24.i25.2661
17. Thomas JA, Kendall BJ, El-Serag HB, et al. Hepatocellular and extrahepatic cancer risk in people with non-alcoholic fatty liver disease. *Lancet Gastroenterol Hepatol*. 2024;9(2):159–169. doi:10.1016/S2468-1253(23)00275-3
18. Spacek L. Clinical guidelines on nonalcoholic fatty liver disease. *JAMA*. 2024;331(12):1062–1063. doi:10.1001/jama.2024.0948
19. Casirati E, Valenti L. SLC7A11 transporter maintains critical nonessential amino acids levels to hamper ferroptosis during MASLD progression. *Sci Bull*. 2023. doi:10.1016/j.scib.2025.01.014
20. Xie C, Jiang X, Yin J, et al. Bisphenol S accelerates the progression of high fat diet-induced NAFLD by triggering ferroptosis via regulating HMGCS2. *J Hazard Mater*. 2023;487:137166. doi:10.1016/j.jhazmat.2025.137166
21. Wang L, Yu H, Wang D, et al. Diosgenin alleviates lipid accumulation in NAFLD through the pathways of ferroptosis defensive and executive system. *J Nutr Biochem*. 2023;140:109886. doi:10.1016/j.jnutbio.2025.109886
22. Doll S, Freitas FP, Shah R, et al. FSP1 is a glutathione-independent ferroptosis suppressor. *Nature*. 2019;575(7784):693–698. doi:10.1038/s41586-019-1707-0
23. Lu D, Xia Q, Yang Z, et al. ENO3 promoted the progression of NASH by negatively regulating ferroptosis via elevation of GPX4 expression and lipid accumulation. *Ann Transl Med*. 2021;9(8):661. doi:10.21037/atm-21-471
24. Yang WS, SriRamaratnam R, Welsch ME, et al. Regulation of ferroptotic cancer cell death by GPX4. *Cell*. 2014;156(1–2):317–331. doi:10.1016/j.cell.2013.12.010
25. Kagan VE, Mao G, Qu F, et al. Oxidized arachidonic and adrenic PEs navigate cells to ferroptosis. *Nat Chem Biol*. 2017;13(1):81–90. doi:10.1038/nchembio.2238
26. Toyokuni S. Iron and thiols as two major players in carcinogenesis: friends or foes? *Front Pharmacol*. 2014;5:200. doi:10.3389/fphar.2014.00200
27. Safe S, Kothari J, Hailemariam A, et al. Health benefits of coffee consumption for cancer and other diseases and mechanisms of action. *Int J Mol Sci*. 2023;24(3). doi:10.3390/ijms24032706
28. Mishima E, Nakamura T, Zheng J, et al. DHODH inhibitors sensitize to ferroptosis by FSP1 inhibition. *Nature*. 2023;619(7968):E9–E18. doi:10.1038/s41586-023-06269-0